# The Unusual Southern Hemisphere Stratosphere Winter of 2002

PAUL A. NEWMAN

NASA Goddard Space Flight Center, Greenbelt, Maryland

ERIC R. NASH

Science Systems and Applications, Inc., Landover, Maryland

Submitted 14 May 2003.

*Corresponding author address:* Paul A. Newman, Mail Code 916, NASA Goddard Space Flight Center, Greenbelt, MD 20771.

E-mail: newman@code916.gsfc.nasa.gov

ABSTRACT

The Southern Hemisphere stratospheric winter of 2002 was the most unusual winter yet observed in the Southern Hemisphere climate record. Temperatures near the edge of the Antarctic polar vortex were considerably warmer than normal over the entire course of the winter. The polar night jet was considerably weaker than normal, and was displaced more poleward than has been observed in previous winters. These record high temperatures and weak jet resulted from a series of wave events that took place over the course of the winter. The propagation of these wave events from the troposphere is diagnosed from time series of Eliassen-Palm flux vectors. The propagation was forced by strong levels of planetary wave 1 in the midlatitude lower troposphere and a low index of refraction at the tropopause. The wave events tended to occur irregularly over the course of the winter, and preconditioned the polar night jet for the extremely large wave event of 22 September. This large wave event resulted in the first ever observed major stratospheric warming in the Southern Hemisphere. This wave event split the Antarctic ozone hole. The combined effect of the wave events of the 2002 winter resulted in the smallest ozone hole observed since 1988.

## 1. Introduction

During the fall of 2002, the Antarctic ozone hole was unusually disturbed (Stolarski et al. 2003, manuscript submitted to *J. Atmos. Sci.*). First, the ozone hole was considerably smaller than has been observed during early September. Second, the ozone hole split into two parts on 22 September 2002. This unusual behavior was not a result of changing chlorine levels, but because of the stratospheric temperature and dynamics that occurred over the winter. There are two necessary conditions for causing the Antarctic ozone hole: high levels of halogens (specifically chlorine and bromine, see WMO 1995), and temperatures cold enough to form polar stratospheric clouds (PSCs).

The impact of temperature on Antarctic ozone losses has always been considered to be of secondary importance because temperatures are always cold enough to form extensive PSCs, and the Southern Hemisphere has small interannual variability during winter (Randel 1992). It has long been recognized that Antarctic September temperatures exhibit extremely cold conditions (i.e., temperatures $< 193$ K, the approximate formation temperature for PSCs). For example, Court (1942) noted the very cold winter conditions from balloon observations during September 1940 at Little America (78°S) and remarked "... since in general, soundings ended prematurely as soon as they reached -80°C level, apparently the limit of balloon elasticity." In contrast, Arctic temperatures are both warmer and more variable. This variability occasionally results in large Arctic ozone losses (e.g., 1997), or virtually no ozone loss at all (e.g., 1999) (Rex et al. 2002).

This unusual winter challenges our understanding of the Southern hemisphere stratosphere, viz., the Southern Hemisphere stratosphere is typically very cold because wave forcing is weak. The occurrence of such a winter could be driven by internal processes, or possibly climate change effects. Our ability to predict future Antarctic ozone levels is constrained by our understanding of the dynamics and climate forcings that control the stratospheric temperatures in the Antarctic stratosphere. Hence it is extremely important to understand why the winter of 2002 was so unusual. Therefore, it is necessary to (1) understand

the morphology of this winter's evolution in contrast to climatology, (2) describe the sequence of wave events over the course of the winter, and (3) understand the formation and propagation of these events.

This paper will describe the evolution of the 2002 SH stratospheric winter. First, the winter of 2002 evolved from a larger than normal series of wave events that spanned the entire winter. These waves varied in strength and duration, with the largest and most spectacular being the major warming of 22 September 2002 that split the ozone hole into two pieces (Thompson 2003, manuscript submitted to *Science*). Second, each wave event acted to warm the region near the polar night jet, i.e., the winter was characterized by a series of minor and a single major warming. The total wave energy propagating into the stratosphere quantitatively explains the much warmer than normal temperatures during September. Third, the polar vortex broke down earlier than normal. The typical warming of the SH has a regular downward progression that usually begins in July in the upper stratosphere and ends in late November in the lower stratosphere. In 2002, this same downward progression of warming also occurred, but at an accelerated rate because of the greater number of wave events over the course of the winter. Fourth, eddy variance in the troposphere was large, but did not exhibit a systematic pattern over the winter. However, the wave 1 pattern was clearly anomalous during the winter of 2002 from the tropics to the high latitudes.

## 2. Data

The National Centers for Environmental Prediction/National Center for Atmospheric Research reanalysis (NNR) data are used as the basis for this work. These analyses are restricted to data after 1978 because of the poorer quality of the NNR data in the stratosphere prior to the inclusion of satellite observations in 1979 (Mo et al. 1995; Kanamitsu 1997; Santer et al. 1999; Marshall 2002). In addition, certain quantities calculated, such as the heat flux, exhibit considerable uncertainty in both hemispheres (Newman and Nash 2000; Randel et al. 2002). Northern Hemisphere flux values from a variety of analyses show differences of $\pm$15%

(Newman and Nash 2000), while a comparison of the SH heat flux between the NNR and European Centre for Medium-Range Weather Forecasts analyses by Randel et al. (2002) show large differences. Nevertheless, the differences between the year 2002 and the climatology are large compared to the overall analysis errors. Unless otherwise noted, for display purposes the time series shown herein have been smoothed to reduce day-to-day variability.

## 3. Results

Temperatures near the jet axis were higher than normal in the polar stratosphere during the entire winter. The black line in Figure 1c displays the zonal-mean daily temperature at 65°S and 50 hPa during the 2002 winter, while the white line shows the climatological average. Up to the middle of May, temperatures at 65°S (near the core of the vortex) were near normal. There is a slight increase in the middle of May, followed by a relaxation back to normal temperatures until the middle of June. By late June, temperatures were well above normal, and were regularly higher than any values observed at a comparable time over the last 24 years. In late September, the temperature dramatically increased to values that were 15 K warmer than average.

In contrast to the temperatures near the jet axis, temperatures in the core of the vortex (near the South Pole) were only slightly higher than normal over most of the winter. Figure 1b displays the minimum daily temperature observed between 50°–90°S at 50 hPa during the 2002 winter. Again, the white line shows the average minimum temperature. Only in late September does the temperature jump to a value that is higher than climatology.

Temperatures at higher altitudes inside the vortex were slightly colder than average during the winter. Figure 1a displays the minimum daily temperature observed between 50°–90°S at 10 hPa during the 2002 winter. At these higher altitudes, the 2002 temperatures were generally below the climatological daily average (white line). The exceptions occur in early September and late September through October. These colder than normal temperatures at higher altitudes suggest that PSCs may have been forming at altitudes much higher than

normal during the 2002 winter.

The vertical structure of these warmer than normal temperatures near the edge of the vortex are displayed in Figure 2a. This figure is a height-time plot of the 2002 SH zonal-mean temperature departures from the 1979–2001 mean near the core of the polar night jet (55°–75°S). During April to early May, temperatures are near normal. A minor warming occurs in the middle of May. By early June, temperatures begin to steadily increase with respect to the climatological average. By early July, these temperatures have increased to extremely high values, with further increases culminating in a major stratospheric warming on 22 September 2002. A major warming is defined by a reversal of the zonal-mean temperature gradient between 50°–80°S, combined with a reversal of the very strong 60°S zonal wind at 10 hPa to easterlies. The temperature differences from climatology became increasingly warmer over the course of the winter as a result of stepwise warming, with some cooling after each warming. The warming appears to descend over the course of the winter. For example, the May and June warmings peak near or above 10 hPa, and only extend down to about 100 hPa, the August temperature anomalies peak below 10 hPa and extend below 100 hPa, and the September major warming peaks near 30 hPa and extends below 300 hPa.

The warming of the polar vortex collar region is directly controlled by the planetary waves that propagate upward from the troposphere into the stratosphere (Hartmann et al. 1984; Shiotani and Gille 1987). The black line in Figure 2b is a 2002 time series of midlatitude eddy heat flux at 100 hPa for waves 1–3. As discussed in Andrews et al. (1987), the heat flux represents the vertical flux of wave energy. Over the course of May–October, there are 11 significant wave events (Table 1). Vertical lines are superimposed between panels of Figure 2 to show the connection between the wave events and the warmings. The wave events are irregularly spaced with about a 1–3 week periodicity.

The 2002 wave events are extremely large compared to the climatological average (white line). The gray shading shows the range of these daily values over 1979–2001. The wave events of 8 July, 18 August, and 22 September are all record wave events. The 22 September

event is clearly unprecedented. Further, the level of the eddy heat flux is higher than the climatological average for a considerable fraction of the winter.

The waves not only impact temperature, but also the zonal-mean wind. Figure 2c displays the height-time plot of the zonal-mean zonal wind difference between 2002 and a 1979–2001 average over 20°–90°S. This figure effectively represents the deviation of the average polar night jet strength from climatology. Each wave noted in Figure 2b impacts the strength of the jet in Figure 2c, with the 22 September wave completely reversing the westerlies to weak easterlies. Combined with the temperature increase in Figure 2a and Figure 1, it is clear that this event was the first major stratospheric warming yet observed in the SH. However, it is important to recognize that the flow was first disturbed by the 15 May event, and was highly disturbed by mid-August.

The wave events over the course of the winter cumulatively acted to warm the polar lower stratosphere. Furthermore, this warming is fairly consistent with previous winters. Figure 3a displays the late-September polar temperature at 50 hPa plotted against the average midlatitude heat flux for a 53-day period, consisting of 45 days prior to the first day of the temperature period and overlapping into the temperature period by 8 days. The two quantities are highly correlated. In essence, the cumulative effect of the waves over August–September acts to warm the polar region (see Newman et al. 2001 for a discussion of comparable effects in the Arctic). During 2002, the late-September temperatures were significantly warmer than any previous winter because of the unusual strength and duration of the wave events. Most of the impact of these wave events tends to occur near the edge of the vortex (near the jet axis). While the wave events are apparent in the core of the vortex (see Figure 1a), the effect is smaller than at the edge.

The cumulative effect of the waves also impacted the temperatures prior to the major warming shown in Figure 2a. Figure 3b displays the early-September polar temperature at 50 hPa plotted against the average midlatitude heat flux for a 53-day period prior to this temperature period. Again, note the excellent correlation. Early September 2002 had the

highest temperature with the highest midwinter heat flux. While the 1986 heat flux was comparable to 2002, the flux in early winter was smaller than in 2002. The major difference between 1986 and 2002 was the late-September 2002 major warming. The average heat flux in 2002 changes by about 5 km $s^{-1}$ by shifting the time average by 15 days, an indicator of the magnitude of the late-September 2002 wave event.

The spatial pattern of warm temperatures covers a considerable region of the SH by late August. However, as mentioned previously, the warmer than normal temperatures were predominantly in the region near the jet core. Figure 4a shows temperature differences between July 2002 and a 1979–2001 climatology. The climatology is superimposed on the figure as white lines. Temperatures are much warmer than normal near the climatological jet core and vortex edge. In the vortex core near the pole, temperatures are only 1–2 K warmer than climatology in the lower stratosphere, in agreement with the minimum temperatures shown in Figure 1b. In addition, the temperatures at higher altitude (above 20 hPa) inside the vortex were colder than normal, in agreement with the minimum temperatures shown in Figure 1a.

The zonal-mean wind was also very disturbed during July 2002, prior to the 22 September major warming. Figure 4b displays zonal-mean wind differences between July 2002 and climatology. The jet core was closer to the pole during 2002, and so the polar vortex was somewhat smaller. The zero-wind line in the lower to middle stratosphere was approximately 6°–10° closer to the pole in 2002 than the climatological average. The quasi-biennial oscillation (QBO) was in the westerly phase in 2002, as is apparent from the positive anomaly near the equator at 20–30 hPa. In addition, winds in the upper-stratospheric tropics were in the easterly phase (not shown on Figure 4b). The series of wave events shown in Figure 2b decelerated the jet as shown in Figure 2c, leading to the smaller and weaker vortex by July and into September.

The Eliassen-Palm (EP) flux is an extremely useful diagnostic for evaluating the propagation of waves in the stratosphere. The EP flux vector $\mathbf{F} = (0, F^{(\phi)}, F^{(z)})$ points in the

direction of the wave's group velocity (Andrews et al. 1987). The EP flux is related to the eddy heat and momentum fluxes by

$$F^{(\phi)} = \rho_0\, a \cos\phi\, (\bar{u}_z\, \overline{v'\theta'}/\bar{\theta}_z - \overline{v'u'}) \quad (1)$$

$$F^{(z)} = \rho_0\, a \cos\phi \{[f - (a\cos\phi)^{-1}(\bar{u}\cos\phi)_\phi]\overline{v'\theta'}/\bar{\theta}_z - \overline{w'u'}\} \quad (2)$$

where $\rho_0$ is the density, $a$ is the earth's mean radius, $\phi$ is the latitude, $z$ is log-pressure height, $(u, v, w)$ are the zonal, meridional, and vertical wind components, $\theta$ is the potential temperature, $f$ is the Coriolis parameter, $\overline{v'\theta'}$ is the eddy potential temperature flux (scaled by a pressure function to obtain the heat flux), $\overline{v'u'}$ is the horizontal eddy momentum flux, the overbar denotes zonal-mean quantities, the prime indicates departures from the zonal mean, and subscripts indicate derivatives with respect to the variable indicated. The term involving the vertical eddy momentum flux $\overline{w'u'}$ has been ignored in our calculations.

The EP flux is shown as a function of altitude and time (Figure 5a), and latitude and time for 300 hPa (Figure 5b) and 10 hPa (Figure 5c). These EP flux vectors are calculated from waves 1-3 (i.e., planetary scales). The vertical lines indicate the major wave events diagnosed from the 100-hPa heat flux, as shown in Figure 2b. The top panel shows that over the winter, these waves are propagating into the stratosphere from the lower to middle troposphere. Generally the waves move upward and equatorward. Equatorward propagating vectors are shown in black, while poleward vectors are displayed in red. At 10 hPa, these waves are strongly propagating towards the equator. Prior to the middle of May, these planetary-scale waves do not appear to propagate into the stratosphere. Further, after the 22 September event, the waves also do not penetrate into the middle stratosphere, except for weak event in late October. This late-October event produces the final warming that ended the winter.

In the 150–200 hPa region of the stratosphere, the waves generally propagate upward and equatorward (see Figure 5a). The large exception to this case occurs in September during the major warming. A close inspection of Figure 5a shows that the waves are strongly propagating towards the pole over a broad altitude region extending into the middle stratosphere. This

convergence into the polar cap produces the sudden warming by rapidly decelerating the mean wind and warming the polar region. Further examination of the figure shows that the poleward propagation of this 22 September wave extends well into the troposphere.

As noted above, the wave event of 22 September showed propagation into the polar region over a very large vertical depth. Figure 5b displays the EP flux vectors on the 300-hPa surface. On this figure, vectors pointing towards the left are upward propagation, while vectors pointing up are propagating equatorward. This figure shows that the upward propagation of waves in the upper troposphere occurs over a broad latitudinal extent (35°–65°S). Furthermore, nearly all of the wave events at 300 hPa show some poleward wave propagation.

The wave events shown in Figure 2b did not exhibit a particularly coherent pattern over the course of the winter. For example, the wave flux events shown in Figure 2b are computed using only waves 1–3. Table 1 shows the dominant wave numbers associated with each warming. The wave events of 15 May, 8 July, 18 August, and 26 October were all dominated by strong wave 1 patterns, while the 9 June, 31 July, and 5 September events were dominated by wave 2 patterns. While the eddy heat flux is dominated by waves 1 and 2, wave 3 cannot be neglected.

The eddy variability for the winter of 2002 is illustrated in Figure 6. Figure 6a displays the rms wave amplitude as a function of altitude averaged over 45°–75°S for waves 1–3. The rms amplitude has been normalized by the square root of the density to emphasize the tropospheric wave activity. Again, the vertical lines indicate the peak heat flux times at 100 hPa shown in Figure 2b. The figure shows that the heat flux peaks are typically accompanied by coherent waves from the middle troposphere to 10 hPa, as was also shown in Figure 5a. Peak amplitudes at 300 hPa typically precede the peak amplitudes at 10 hPa by a few days. In the stratosphere, the wave amplitudes steadily strengthen over the course of the winter, reaching a maximum during the major warming in late September. The wave events also appear to conserve their amplitudes as they propagate upward. The waves amplitudes are generally a maximum in the troposphere, with a minimum above the tropopause, and a second

maximum in the middle to upper stratosphere.

The planetary-scale eddy variability in the troposphere is concentrated in the 45°–75°S region. Figure 6b shows the rms wave amplitude for waves 1–3 at 300 hPa in the geopotential height field. The wave-event maxima vary in both strength and latitude location over the course of the winter. A Hovmöller diagram of the wave 1–3 eddy field is shown in Figure 6c for a latitude of 60°S (gray horizontal line in Figure 6b). Note that the Hovmöller diagram is dominated by a wave 1 pattern, with the wave 1 peak centered at about 130°W (260 °E), just west of the Antarctic Peninsula. However, it is clear that the wave events primarily occur as episodic bursts of wave energy moving into the stratosphere on a 1–2 week time scale.

Height and streamfunction field deviations from a 1979–2001 climatology in the upper troposphere for June–August (not shown) suggest a possible wave train that is forced in the maritime continent region of the Western Pacific. Correlations of 100-hPa heat flux averages with the midwinter flow field suggests a relationship, viz., strong anticyclonic flow to the west of the Antarctic peninsula (approximately 60°S, 130°W) is associated with large eddy activity propagation into the stratosphere after propagating southward from the tropical upper troposphere.

The height of wave 1 in the streamfunction field is an excellent indicator of the episodic waver behavior of the southern hemisphere during 2002. The streamfunction is derived from the nondivergent components of the NNR wind fields on pressure surfaces and is normalized by the radius of the Earth. Figure 7 shows the streamfunction amplitude of wave 1 over the course of the season as plotted against latitude. Again, the large wave events (as noted in Table 1) are plotted as the partially transparent white vertical lines. The strong wave 1 events of 15 May, 8 July, 18 August, 22 September, and 26 October are all associated with larger than normal wave amplitudes in the 55°–70°S region. These episodes of strong wave 1 are also accompanied by strong wave events that occur in the 10°–25°S region (equatorward of the subtropical jet). However, the events in the 10°–25°S region typically occur a few days prior to the high latitude events. Furthermore, the wave 1 events in the southern tropics are

associated with strong wave 1 events in the northern tropics. This northern tropical wave 1 tends to also precede the southern maximum by a day or so. Hence, the wave 1 events in the southern stratosphere appear to be associated with wave events that develop in the tropics and propagate southward.

We have investigated the propagation of the planetary-scale waves using a cross-correlation analysis of the streamfunction. A cross-correlation analysis of the geopotential height field was used by Randel (1987) to investigate the propagation of planetary waves in the winters of 1983 and 1984. Figure 8 displays the coherence for wave 1 at 60°S and 100 hPa with wave 1 at various other altitudes and time lags. The coherence is effectively the correlation of wave 1 with other altitudes and times. We calculate this coherence using the period 1 May to 15 September 2002. This period is chosen to understand the wave 1 events prior to the late-September major warming. The strong coherence between the troposphere and 100 hPa is evident, but shows a shift backward of 2–3 days down to the surface. In addition, the peak of the coherence shifts forward in time at 10 hPa by about 2 days. This tilt of the coherence is directly related to the upward propagation of wave 1, with a wave propagation of approximately 6 km day$^{-1}$. Plots for waves 2 and 3 show similar coherence, but with faster vertical propagation. This coherence pattern is in good agreement with the EP flux propagation shown in Figure 5, and confirms the time lag in the wave events between the middle troposphere and middle stratosphere.

We can further trace the behavior of waves in the middle to lower troposphere using wave 1 coherence plots with various time lags. Figure 9 displays the coherence between the 150 hPa and 30°S point and all of the points on a latitude vs. pressure-altitude plot for time lags of -4, 0, +2, and +4 days. This figure shows the coherence of the tropical wave 1 pattern with the midlatitude lower tropospheric wave 1. The pattern indicates strong coherence across the upper tropospheric tropics from 20°N to 30°S (Figure 9a) at a -4-day lag. This suggests cross-equatorial wave propagation (as indicated by the arrow). The 0-day and +2-day lag panels (Figure 9b and c) show a correlation of the upper-tropospheric subtropics (30°S)

has developed with wave 1 at 700 hPa and 55°S (indicated by the arrows). The +4-day lag panel (Figure 9d) shows a weakening wave 1 in the tropics, with intensifying coherence from 700 hPa into the stratosphere at 60°S. This figure shows that the stratospheric wave 1 pattern is strongly influenced by a tropical wave 1 on a time scale of about 8 days.

Because of the strong coherence between wave 1 at 150 hPa and wave 1 at 700 hPa 2–3 days earlier, we have examined the long term behavior of the streamfunction at 700 hPa. Figure 10a displays the average wave 1 amplitude between 50°–70°S at 700 hPa for each year from 1979–2002 for a 1 May to 15 September average. In this figure, 2002 stands out as the record value. In addition, 1988 and 1992 also stand out as maxima, and these were also years with active ozone holes. As noted above, the wave 1 amplitude at 700 hPa is related to the tropical wave 1 amplitude with about a 4-day lag. Figure 10b displays the average wave 1 amplitude between 10°–20°S at 300 hPa for each year from 1979–2002 for the same 1 May to 15 September average (no time lag). Again, the wave 1 amplitude in the southern tropics is a maximum. The two time series have a reasonable 0.51 correlation, which for 24 years that are independent this is significantly different from zero at the 99% confidence level for a 2-sided Student's *t* test. However, this correlation only explains about 26% of the variance in the wave 1 700-hPa variance.

We have also examined the coherence of waves 2 and 3 during the winter of 2002. Both waves 2 and 3 shows distinct vertical propagation into the stratosphere, but only a weak relationship to the subtropics.

## 4. Discussion

The SH stratosphere was extremely disturbed during the winter of 2002. The culmination of this disturbed stratosphere was the major warming of 22 September. There are two hypotheses to explain this increase in stratospheric wave activity: (1) excessive tropospheric wave forcing in 2002 propagating upward into the stratosphere, and (2) an anomalous mean flow that allowed moderate tropospheric waves to more easily propagate into the stratosphere.

The tropospheric wave forcing was higher than average during the 2002 winter. For April–September, the 200-hPa heat flux for waves 1–3 between 40°–70°S was 50% stronger than climatology, and substantially stronger than any previous year. If we exclude September from this average, then the heat flux was still about 40% stronger than climatology, but comparable to both 1992 and 1995. While it was higher than average, wave forcing was not at record levels near the tropopause. However, as was shown in Figure 10a, wave 1 was anomalously larger in the lower troposphere. This higher than normal wave 1 is related to higher than normal wave 1 in the tropics. Both waves 2 and 3 were also higher than normal in 2002, but did not show any relationship to tropical wave forcing.

As noted above, wave 1 in the lower troposphere was stronger than normal during the winter of 2002. From the coherence in Figure 9, wave 1 at this subtropical point is strongly related to northern subtropical waves. This suggests that wave energy propagates southward across the equator and downward into the southern midlatitude troposphere, reinforcing the wave 1 in the lower troposphere, which then propagates upward into the stratosphere.

The weaker stratospheric winds and warmer temperatures seen in 2002 are clearly consistent with greater wave forcing (e.g., the modeling study of Taguchi and Yoden 2002). However, the generation of these large-scale stratospheric waves is quantitatively difficult to explain. Large wave forcing from the SH troposphere is consistent with the modeled dynamic forcing discussed in Scinocca and Haynes (1998). In their model, stratospheric wave activity was forced by nonlinear wave-wave interaction of tropospheric baroclinic waves. This wave-wave interaction was characterized by waves with relatively slow phase velocities embedded in wave packets with large group velocities. However, they noted that it was not always possible to associate forcing of waves with bursts of upward EP flux. The upper tropospheric eddies do not show clear evidence of excessively strong wave packets.

The wave propagation is controlled by the index of refraction, which is proportional to the meridional potential vorticity gradient and inversely proportional to the zonal-mean wind minus the wave's phase speed (Dickinson 1968). As was noted in Figure 2b, the zero-wind

line was 6°–10° closer to the pole in 2002. At 10 hPa, the 20 m $s^{-1}$ zonal-mean wind is usually found at 36.4°S. In 2002, the 20 m $s^{-1}$ zonal-mean wind was found at 43.6°S. During August 2002 (preceding the major warming), the polar-night jet was the weakest yet observed, and the equatorial flank of the jet was located at the most southerly latitude since 1988. This implies that slow-moving planetary waves would encounter a critical line at a more southerly latitude than was normally found in past years. This anomalous jet structure was also found in earlier months of 2002. For example, in April (prior to any wave events noted herein), the subtropical zonal winds in the upper stratosphere were anomalously easterly, and the jet was a few degrees closer to the pole than normal. The structure of the zonal-mean wind during 2002 was anomalous, suggesting that wave propagation was highly anomalous during 2002.

The impact of tropical and extratropical winds on stratospheric variability has been shown by Holton and Tan (1982). They showed that the QBO impacted wave propagation in the NH stratosphere, and hence the interannual variability of the polar vortex. Gray et al. (2001a) extended this work to show that upper stratospheric winds dramatically impacted NH polar vortex variability, while Gray et al. (2001b) utilized a model to show that middle- to upper-stratospheric equatorial winds were necessary to explain the Holton-Tan relationship. Scott and Haynes (1998) have also used a model to demonstrate that disturbed winters are accompanied by late-fall to early-winter easterlies in the subtropics. Indeed, such easterlies were observed in 2002 in the tropics in association with a westerly QBO at 30 hPa. In fact, temperatures near the vortex edge in early September are highly anticorrelated with tropical winds in the upper stratosphere.

In addition to the stratospheric index of refraction, the index of refraction at the tropopause was slightly more conducive to waves propagating into the stratosphere. Chen and Robinson (1992) suggested that the refractive index at the tropopause acted as a valve for the propagation of planetary waves. Figure 11 is a plot of the 45°–75°S 100-hPa heat flux plotted against the quasi-geostrophic potential vorticity (PV) meridional gradient as a function of year, averaged between 400 and 100 hPa and 40°–60°S. The quantities are time

averaged from 1 May to 15 September for each year. The correlation between the heat flux and PV gradient is 0.77. If we perform a multiple regression of the 500-hPa heat flux (tropospheric wave forcing) and the PV gradient (index of refraction) against the 100-hPa heat flux, the correlation increases to 0.9. This is consistent with the hypothesis that the wave energy that has entered the stratosphere is directly related to the tropospheric forcing and the valving near the tropopause controlled by the index of refraction.

## 5. Summary and Conclusions

The 2002 SH winter had perhaps the most interesting stratospheric conditions yet observed since stratospheric observations first began in the 1940s. This winter had the only major stratospheric warming ever observed in the SH. While such major warmings are relatively common in the NH, the typical warming of the SH only occurs in the final warming during October–November. The warmer temperatures and stronger wave dynamics significantly impacted the Antarctic ozone hole.

The 2002 hole was the least severe since 1988. The 2002 wave events dramatically impacted the Antarctic ozone hole ((Stolarski et al. 2003, manuscript submitted to *J. Atmos. Sci.*). Using Total Ozone Mapping Spectrometer ozone, the size of the hole was already small during the period preceding the major warming. This smaller size is consistent with the warmer temperatures at the vortex edge. The major warming then split the Antarctic ozone. The ozone hole had an early disappearance in response to the final wave event on 26 October.

The mean temperature of the polar lower stratosphere was much warmer than normal during the winter of 2002. The temperature of the Antarctic stratosphere was directly related to the wave forcing events observed over the course of the winter. While strong eddy forcing of the SH stratosphere is not common, the resulting high temperatures were generally consistent with this strong forcing in both magnitude and timing. Hence, the higher than normal polar temperatures did not result from any direct radiative forcing mechanism.

The SH stratospheric wind fields were also highly anomalous during the winter of 2002.

This was especially true following the major warming of 22 September. However, it is also clear that the winds were abnormal as far back as April. The anomalous easterlies in the middle to upper stratosphere intensified over the course of the winter, with the jet becoming progressively weaker and moving closer to the pole. The wave events up through early September preconditioned the wind fields to allow the major warming of 22 September.

The stronger than normal wave 1 appears to result from strong forcing of wave 1 in the tropics of both the NH and SH. First, the stratospheric wave 1 observed during 2002 is directly tied to the lower troposphere with a 2-day lag, and this wave 1 in the lower troposphere is highly correlated to the tropical wave 1. Second, EP flux diagrams show wave propagation from the subtropical jet poleward, followed by upward propagation into the stratosphere. Third, the 2002 winter average wave 1 amplitudes in both the midlatitude lower troposphere and tropical upper troposphere were the largest values observed in the 24-year record. While the EP flux and correlation diagnostics provide a strong case for a tropical wave 1 forcing, the magnitude of the EP flux in the stratosphere is excessive in comparison to the tropospheric forcing.

The winter dynamics of 2002 is directly responsible for the unusual ozone hole, and the unusual dynamics appears to result from higher than average wave forcing from the troposphere. In particular, we find that the larger than normal propagation of planetary-scale waves into the stratosphere was caused by 2 main factors: (1) stronger than normal levels of planetary wave 1 in the southern midlatitude lower troposphere, and (2) a propagation state that was conducive to upward propagation of waves (i.e., a lower than normal index of refraction at the tropopause that allowed more wave penetration into the stratosphere, and tropical upper-stratospheric easterlies).

Certain question remain unresolved. First, what is the mechanism for the forcing of the tropical wave 1? Correlation with sea surface temperatures and the southern oscillation index do not show significant correlations with the tropical wave 1 in the upper troposphere. Australia experienced a severe drought and the monsoon rainfall

was 19% below normal during 2002 (NOAA/NCDC Climate of 2002 Annual Review, http://lwf.ncdc.noaa.gov/oa/climate/research/2002/ann/ann02.html). The 2002 El Niño was also anomalous, with the warm SST anomaly located in the Central rather than Eastern Pacific (Michelle Reinecker 2003, private communication). Such anomalous behavior in both these dry regions and El Niño behavior suggest an unusual forcing of large-scale waves in the tropics during 2002. Second, why were waves 2 and 3 amplitudes and heat fluxes unusually high, but not in the tropics? From Hovmöller diagrams and coherency plots, a traveling wave 2 pattern is evident over most of the winter with a period of 10–14 days. However, the forcing of this traveling Rossby wave 2 is not apparent. The unusual wave 2 and 3 patterns may be caused by wave trains forced in the tropics and propagating into the midlatitudes as was shown shown in Hoskins and Karoly (1981) for the NH winter. Third, what are the factors that control upward wave propagation in the SH midlatitudes? To first order, conventional Charney-Drazin theory explains vertical wave propagation. However, in midwinter, some planetary-scale waves amplify and propagate upward while other waves do not. Hence, what other factors control vertical propagation from the troposphere to the stratosphere?

To briefly summarize, planetary wave 1 events were forced in the tropical upper troposphere. These tropically-forced waves occurred episodically over the course of the SH winter. They took 2–4 days to propagate across the equatorial region and downward into the lower troposphere near 55°S. Because the zonal-mean flow at the tropopause and in the tropical upper stratosphere was conducive to wave propagation, the planetary-scale waves in the lower troposphere were efficiently refracted upward into the stratosphere. Over the course of the winter, there was a series of planetary waves that propagated upward from the troposphere into the stratosphere. These wave events warmed the polar lower stratosphere and weakened the jet stream. By the middle of September, the wave events had preconditioned the stratospheric zonal-mean wind pattern to allow the occurrence of a major warming. A large event on 22 September then resulted in a major warming of the stratosphere. This warming was strong enough to warm temperatures beyond the formation point for polar stratospheric

clouds, thereby stopping ozone loss.

*Acknowledgments.* We wish to thank Drs. Darryn Waugh, Warrick Norton, Mark Schoeberl, Lorenzo Polvani, Lesley Gray, and Matthew Hitchman for helpful discussions. This work was supported under a NASA grant from the Atmospheric Chemistry, Modeling, and Analysis Program. Sea surface temperatures and the southern oscillation index provided by the NOAA NCEP Climate Prediction Center.

REFERENCES

Andrews, D. G., J. R. Holton, and C. B. Leovy, 1987: *Middle Atmosphere Dynamics.* Academic, San Diego, Calif., 489 pp.

Chen, P., and W. A. Robinson, 1992: Propagation of planetary waves between the troposphere and stratosphere. *J. Atmos. Sci.,* **49**, 2533–2545.

Court, A., 1942: Tropopause disappearance during the Antarctic Winter. *Bull. Amer. Met. Soc.,* **23,** 220–238.

Dickinson, R. E., 1968: Planetary Rossby waves propagating vertically through weak westerly wind wave guide. *J. Atmos. Sci.,* **25,** 984–1002.

Gray, L. J., E. F. Drysdale, T. J. Dunkerton, and B. N. Lawrence, 2001a: Model studies of the interannual variability of the Northern Hemisphere stratospheric winter circulation: The role of the quasi-biennial oscillation. *Quart. J. Roy. Met. Soc.,* **127,** 1413–1432.

_____, S. J. Phipps, T. J. Dunkerton, M. P. Baldwin, E. F. Drysdale, and M. R. Allen, 2001b: A data study of the influence of the equatorial upper stratosphere on Northern Hemisphere stratospheric sudden warmings. *Quart. J. Roy. Met. Soc.,* **127,** 1985–2003.

Hartmann, D. L., C. R. Mechoso, and K. Yamazaki, 1984: Observations of wave-mean flow interaction in the Southern Hemisphere. *J. Atmos. Sci.,* **41,** 351–362.

Holton J. R., and H. C. Tan, 1982: The quasi-biennial oscillation in the Northern Hemisphere lower stratosphere. *J. Meteorol. Soc. Japan,* **60,** 140–148.

Hoskins, B. J., and D. J. Karoly, 1981: The steady linear response of a spherical atmosphere to thermal and orographic forcing. *J. Atmos. Sci.,* **38,** 1179–1196.

Kanamitsu, M., R. E. Kistler, and R. W. Reynolds, 1997: NCEP/NCAR reanalysis and the use of satellite data. *Adv. Space Res.,* **19,** 481–489.

Marshall, G. J., 2002: Trends in Antarctic geopotential height and temperature: A comparison between radiosonde and NCEP-NCAR reanalysis data. *J. Climate,* **15,** 659–674.

Mo, K. C., X. L. Wang, R. Kistler, M. Kanamitsu, and E. Kalnay, 1995: Impact of satellite data on the CDAS reanalysis system. *Mon. Wea. Rev.,* **123,** 124–139.

Newman, P. A., and E. R. Nash, 2000: Quantifying the wave driving of the stratosphere. *J. Geophys. Res.*, **105,** 12,485–12,497.

_____, _____, and J. E. Rosenfield, 2001: What controls the temperature of the Arctic stratosphere during the spring? *J. Geophys. Res.*, **106,** 19,999–20,010.

Randel, W. J., 1986: A study of planetary waves in the southern winter troposphere and stratosphere. Part 1: Wave structure and vertical propagation. *J. Atmos. Sci.,* **44,** 917–935.

_____, 1992: Global atmospheric circulation statistics, 1000–01 mb. *NCAR Tech. Note, NCAR/TN-366+STR,* 256 pp.

_____, F. Wu, and R. Stolarski, 2002: Changes in column ozone correlated with the stratospheric EP flux. *J. Met. Soc. Japan*, **80,** 849–862.

Rex, M. and Coauthors, 2002: Chemical depletion of Arctic ozone in winter 1999/2000. *J. Geophys. Res.*, **107,** 8276, doi:10.1029/2001JD000533.

Santer, B. D., J. J. Hnilo, T. M. L. Wigley, J. S. Boyle, C. Doutriaux, M. Fiorino, D. E. Parker, and K. E. Taylor, 1999: Uncertainties in observationally based estimates of temperature change in the free atmosphere. *J. Geophys. Res.*, **104,** 6305–6333.

Scinocca, J. F., and P. H. Haynes, 1998: Dynamical forcing of stratospheric planetary waves by tropospheric baroclinic eddies. *J. Atmos. Sci., 55,* 2361–2392.

Scott, R. K., and P. H. Haynes, 1998: Internal interannual variability of the extratropical stratospheric circulation: The low-latitude flywheel. *Q. J. Roy. Meteor. Soc.*, **124,** 2149–2173.

Shiotani, M., and J. C. Gille, 1987: Dynamic factors affecting ozone mixing ratios in the Antarctic lower stratosphere. *J. Geophys. Res.*, **92,** 9811–9824.

Taguchi, M., and S. Yoden, 2002: Internal interannual variability of the troposphere-stratosphere coupled system in a simple global circulation model. Part I: Parameter sweep experiment. *J. Atmos. Sci.,* **59,** 3021–3036.

World Meteorological Organization, 1995: Scientific Assessment of Ozone Depletion: 1994. *Rep. 37,* Global Ozone Res. and Monitor. Proj., Geneva, Switzerland.

**Figure 1.** Daily minimum temperature averaged over 50°–90° S at (a) 10 hPa and (b) 50 hPa. (c) Daily zonal-mean temperature at 65°S and 50 hPa. The black line in each panel shows the 2002 temperature. The white line displays the 23-year average (1979–2001) and is smoothed with a 15-day boxcar. The gray shading indicates the range of values observed between 1979 and 2001. The vertical gray lines passing through all panels indicate the days of maximum eddy heat flux at 100 hPa.

**Figure 2.** (a) Daily temperature departures from the 1979–2001 mean for 1 April to 31 October 2002, averaged for 55°–75°S at 50 hPa. Contour intervals are 2 K and negative contours are dashed. (b) Daily eddy heat flux at 100 hPa, averaged for 40°–70°S. Units are in K m $s^{-1}$. The black line shows the 2002 values, which have been smoothed with a 1-2-1 filter applied 3 times. The white line displays the 23-year average (1979–2001) and is smoothed with a 15-day boxcar. The gray shading indicates the range of values (also 1-2-1 filtered) observed between 1979 and 2001. (c) Daily zonal-mean zonal wind departures from the 1979–2002 mean, averaged for 20°–90°S. Contour intervals are 2 m $s^{-1}$ and negative contours are dashed. The vertical lines passing through all panels indicate the days of maximum eddy heat flux at 100 hPa.

**Figure 3.** Temperature at 50 hPa and averaged for 60°–90°S plotted against eddy heat flux at 100 hPa and averaged for 45°–75°S. (a) Temperature averaged for 16–30 September and eddy heat flux averaged for 2 August to 23 September. (b) Temperature averaged for 1–15 September and eddy heat flux averaged for 18 July to 8 September. The solid line is the least-squares regression fit and the correlations are indicated. Each year is indicated by the last two digits.

**Figure 4.** (a) July zonal-mean temperature departures from the long-term mean (1979–2001). Contour intervals are 1 K. The white contours are the long-term mean field, with intervals of 5 K. (b) July zonal-mean zonal wind departures from the long-term mean (1979–2001). Contour intervals are 2 m $s^{-1}$. The white contours show the long-term mean field, with intervals of 10 m $s^{-1}$. Negative contours are dashed in both panels.

**Figure 5.** (a) Daily Eliassen-Palm (EP) flux vectors for waves 1–3 averaged from 30°–70°S. The vectors have been multiplied by the log of pressure to emphasize the lower altitude values. Vectors pointing up indicate vertical propagation while vectors pointing to the right indicate equatorward propagation. Daily EP flux vectors at 300 hPa (b) and 10 hPa (c). In these lower 2 panels, vectors pointing upward indicate equatorward propagation while vectors pointing to the left indicate upward propagation. In all 3 panels, EP flux vectors less than 20% of the maximum vector over the whole field have not been plotted. The colorscale used indicates black as equatorward pointing and red as poleward pointing.

**Figure 6.** (a) Pressure-time plot of daily geopotential height rms waves 1–3 amplitude averaged over latitudes 45°–75°S. The rms wave amplitude is normalized by the density. The horizontal white line shows the 300-hPa level. Contour intervals are 25 m. (b) Latitude-time plot of daily geopotential height rms waves 1–3 amplitude at 300 hPa. The white horizontal lines indicate the 45°and 75°S lines used in (a), while the horizontal gray line is the 60°S line. Contour intervals are 100 m. (c) Longitude-time plot of daily geopotential height waves 1–3 deviations from the zonal mean at 60°S and 300 hPa. Contour intervals are 300 m. The vertical lines passing through all panels indicate the days of maximum eddy heat flux at 100 hPa.

**Figure 7.** Latitude-time plot of the 300-hPa amplitude of wave 1 derived from the streamfunction. The streamfunction is derived from the nondivergent components of the wind field on pressure surfaces. The streamfunction values are normalized by the radius of the Earth. Units are m $s^{-1}$. The white semi-transparent vertical lines indicate the days of maximum eddy heat flux at 100 hPa.

**Figure 8.** Contour plot of the 100 hPa, 60°S wave 1 coherency plotted as a function of pressure and time lag. Coherency is similar to a correlation coefficient, and represents linearly related temporal variability between points. The white lines are drawn onto the axis of the maximum of the coherency to illustrate the vertical propagation of wave 1. Contour intervals are 0.1.

**Figure 9.** Contour plots of the 150 hPa, 30°S wave 1 coherency plotted as a function of altitude and latitude for phase lags of (a) -4 days, (b) 0 days, (c) +2 days, and (d) +4 days. The white lines are drawn onto the axis of the maximum of the coherency to illustrate the propagation of wave 1. Contour intervals are 0.1.

**Figure 10.** Amplitude of wave 1 streamfunction for 1979–2002 averaged over 1 May to 15 September for each year. (a) Streamfunction at 700 hPa and averaged for 50°–70°S. (b) Streamfunction at 300 hPa and averaged for 10°–20°S.The streamfunction is derived from the nondivergent part of the meridional and zonal winds on pressure surfaces.

**Figure 11.** Eddy heat flux vs. the meridional gradient of the quasi-geostrophic potential vorticity ($Q_y$) averaged over 1 May to 15 September for each year. The heat flux is averaged for 45°–75°S at 100 hPa, while $Q_y$ is averaged for 40°–60°S and 100–400 hPa. The index of refraction is proportional to $Q_y$. The correlation is 0.55. Each year is indicated by the last two digits.

**Table 1.** Significant 2002 wave events as indicated by the 100-hPa eddy heat flux averaged over 40°–70°S.

| Date | NDAYS | TOTAL | W1 | W2 | W3 | WN | ΔT |
|---|---|---|---|---|---|---|---|
| 15 May | 5 | -13.86 | **-7.31** | -4.31 | -2.24 | 1,2 | 2.0 |
| 9 June | 4 | -19.72 | -2.80 | **-14.48** | -2.44 | 2 | 1.2 |
| 24 June | 4 | -16.75 | -4.29 | -5.98 | **-6.47** | 1,2,3 | 1.9 |
| 8 July | 7 | -20.01 | **-12.88** | -5.16 | -1.97 | 1 | 1.8 |
| 19 July | 7 | -14.69 | 1.46 | **-8.96** | -7.19 | 2,3 | 2.4 |
| 31 July | 6 | -26.02 | -5.95 | **-18.29** | -1.79 | 2 | 1.5 |
| 18 August | 6 | -25.41 | **-16.43** | -6.10 | -2.87 | 1 | 9.1 |
| 5 September | 5 | -24.64 | -1.35 | **-22.67** | -0.63 | 2 | 1.7 |
| 11 September | 3 | -15.41 | -0.66 | -6.43 | **-8.31** | 2,3 | 0.6 |
| 22 September | 4 | -70.43 | -25.30 | **-28.31** | -16.82 | 1,2,3 | 4.9 |
| 26 October | 8 | -18.01 | **-18.18** | 0.69 | -0.51 | 1 | -4.3 |

Date = Date when the peak in waves 1–3 eddy heat flux is maximum.

NDAYS = The number of days in an event is determined by the when the sign of the first derivative changes on either side of the peak.

TOTAL, W1, W2, W3 = waves 1-3 , wave 1, wave 2, and wave 3 amplitude of eddy heat flux (K m $s^{-1}$).

WN = Dominant wave number(s) for the event.

ΔT = Difference in 50-hPa temperature departures from the 1979–2001 daily means, averaged over 60°–90°S, between criteria used for NDAYS (K).

# Newman & Nash: Figure 1

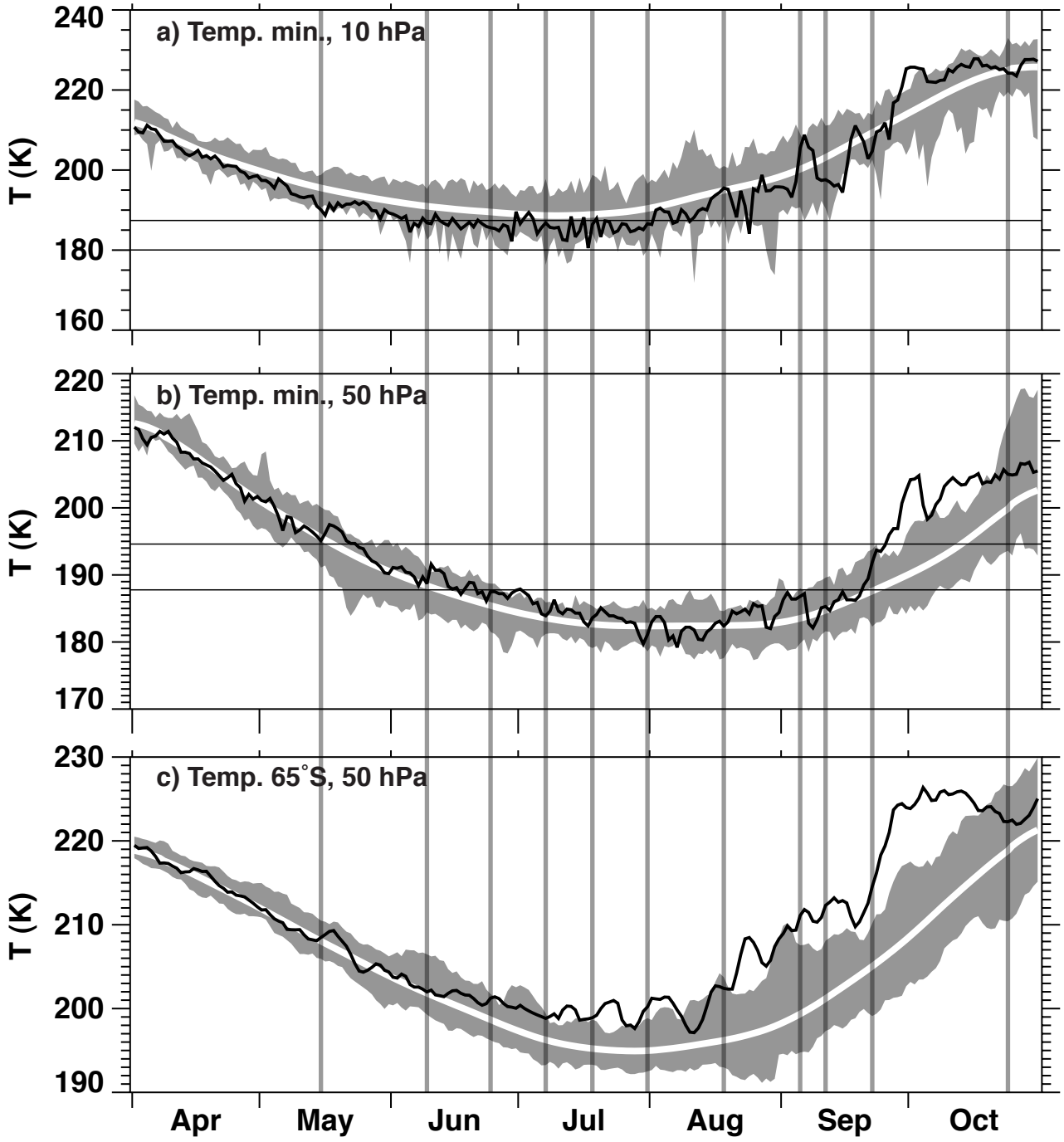


Figure 1. Daily minimum temperature averaged over 50˚–90˚S at (a) 10 hPa and (b) 50 hPa. (c) Daily zonal-mean temperature at 65˚S and 50 hPa. The black line in each panel shows the 2002 temperature. The white line displays the 23-year average (1979–2001) and is smoothed with a 15-day boxcar. The gray shading indicates the range of values observed between 1979 and 2001. The vertical gray lines passing through all panels indicate the days of maximum eddy heat flux at 100 hPa.

# Newman & Nash: Figure 2

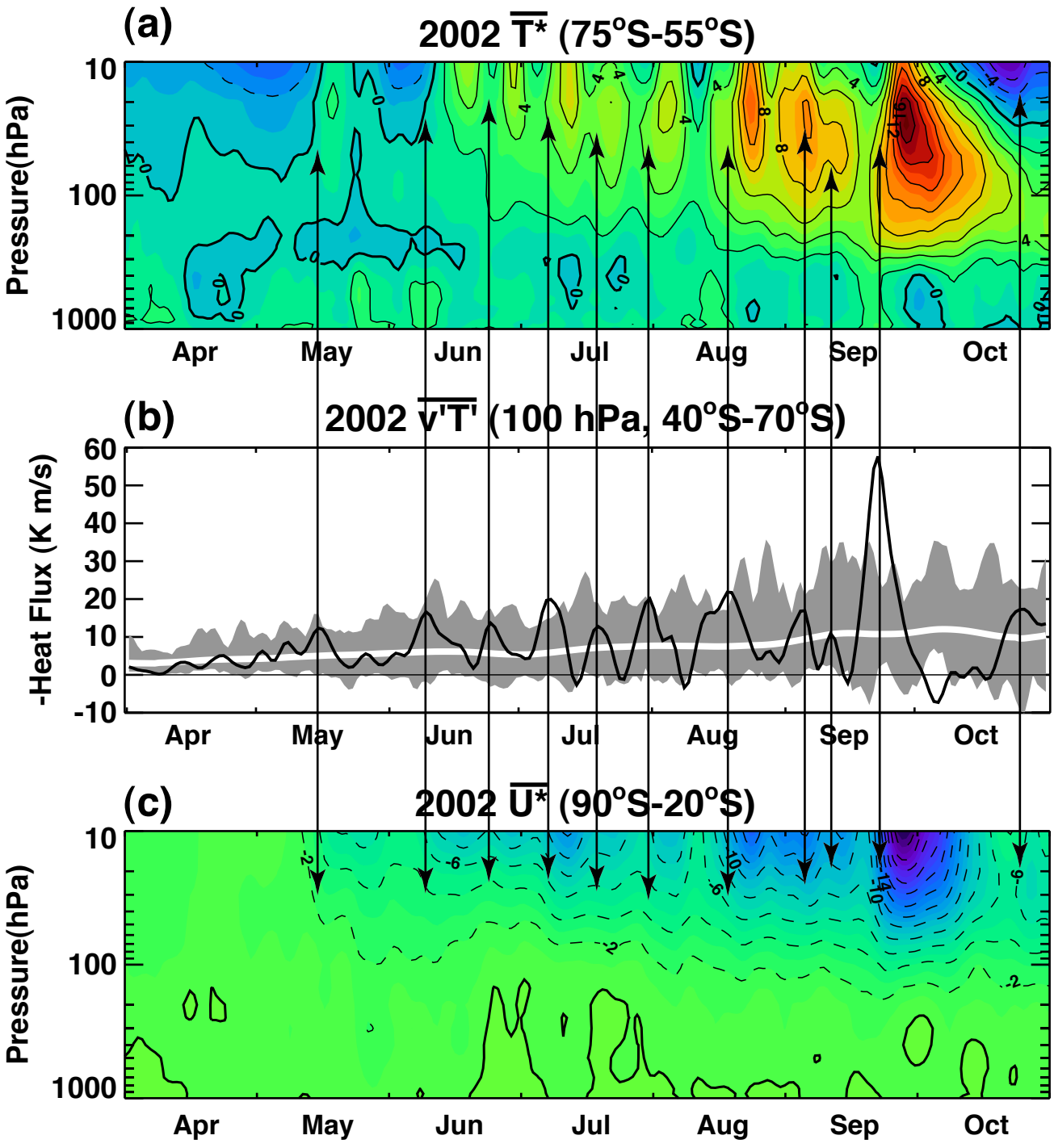


Figure 2. (a) Daily temperature departures from the 1979–2001 mean for 1 April to 31 October 2002, averaged for 55˚–75˚S at 50 hPa. Contour intervals are 2 K and negative contours are dashed. (b) Daily eddy heat flux at 100 hPa, averaged for 40˚–70˚S. Units are in K m s □ . The black line shows the 2002 values, which have been smoothed with a 1-2-1 filter applied 3 times. The white line displays the 23-year average (1979–2001) and is smoothed with a 15-day boxcar. The gray shading indicates the range of values (also 1-2-1 filtered) observed between 1979 and 2001. (c) Daily zonal-mean zonal wind departures from the 1979–2002 mean, averaged for 20˚–90˚S. Contour intervals are 2 m $s^{-1}$ and negative contours are dashed. The vertical lines passing through all panels indicate the days of maximum eddy heat flux at 100 hPa.

# Newman & Nash: Figure 3

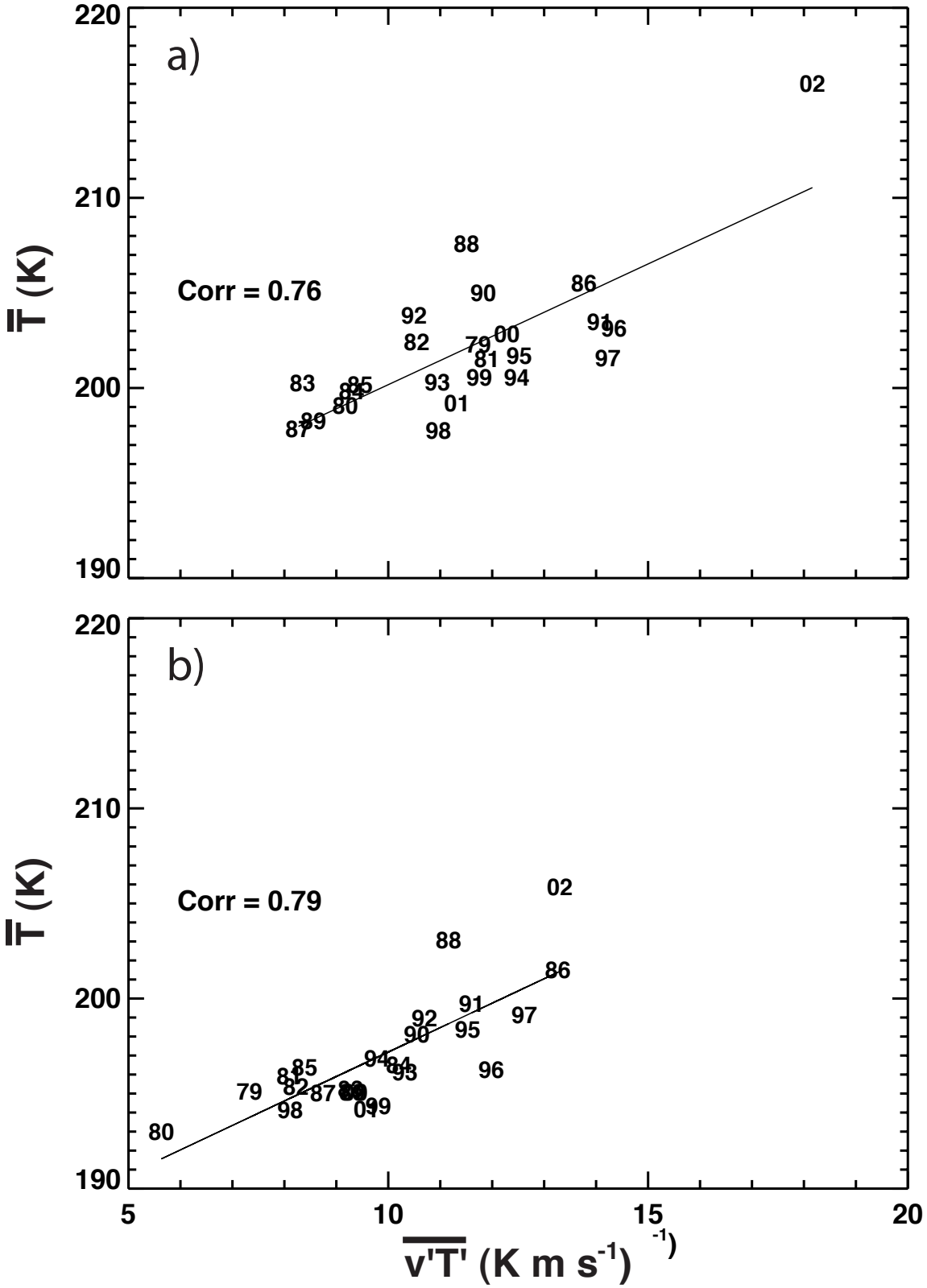


Figure 3. Temperature at 50 hPa and averaged for 60˚–90˚S plotted against eddy heat flux at 100 hPa and averaged for 45˚–75˚S. (a) Temperature averaged for 16–30 September and eddy heat flux averaged for 2 August to 23 September. (b) Temperature averaged for 1–15 September and eddy heat flux averaged for 18 July to 8 September. The solid line is the least-squares regression fit and the correlations are indicated. Each year is indicated by the last two digits.

Newman & Nash: Figure 4

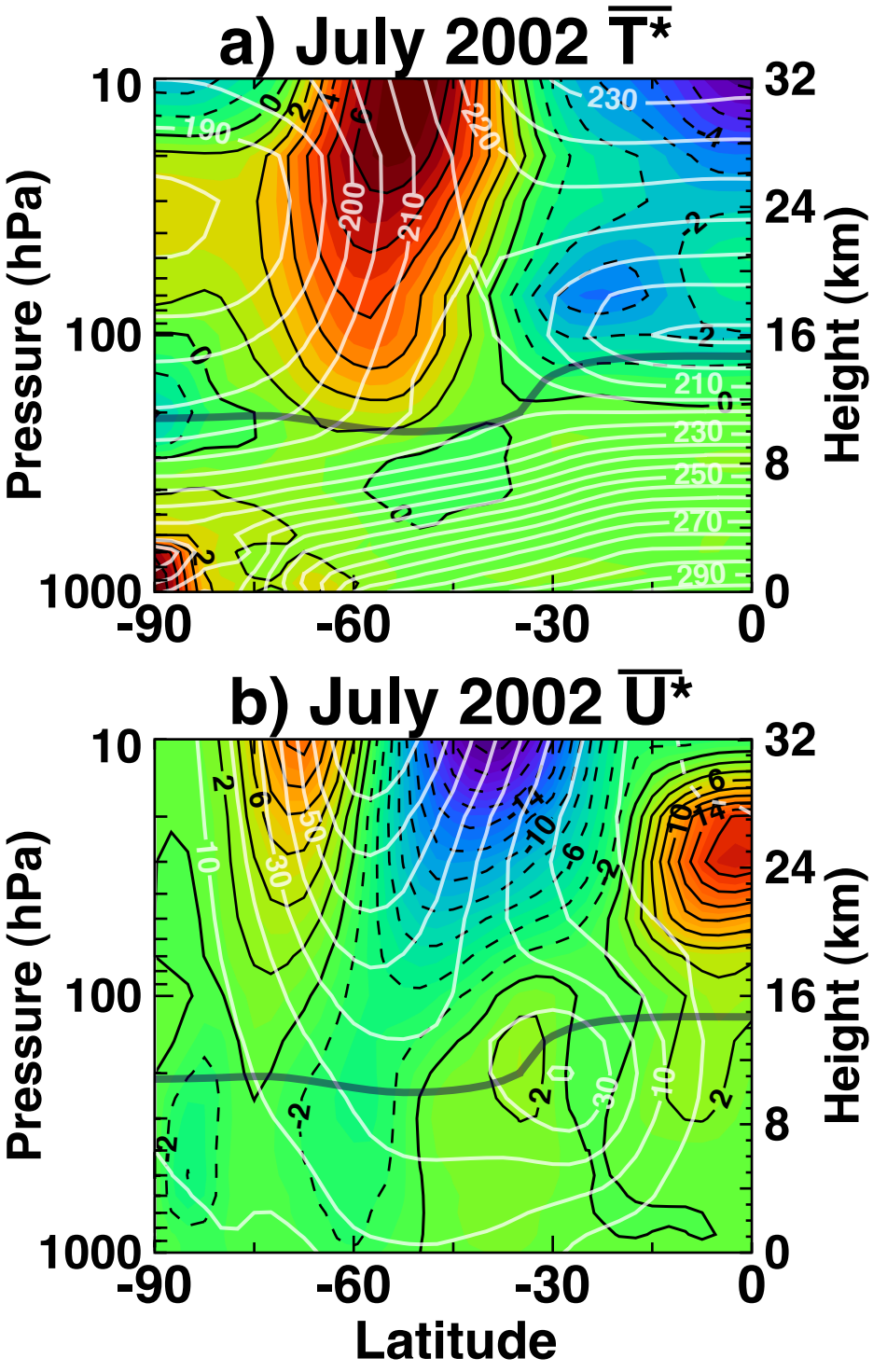


Figure 4. (a) July zonal-mean temperature departures from the long-term mean (1979–2001). Contour intervals are 1 K. The white contours are the long-term mean field, with intervals of 5 K. (b) July zonal-mean zonal wind departures from the long-term mean (1979–2001). Contour intervals are 2 m $s^{-1}$. The white contours show the long-term mean field, with intervals of 10 m $s^{-1}$. Negative contours are dashed in both panels.

# Newman & Nash: Figure 5

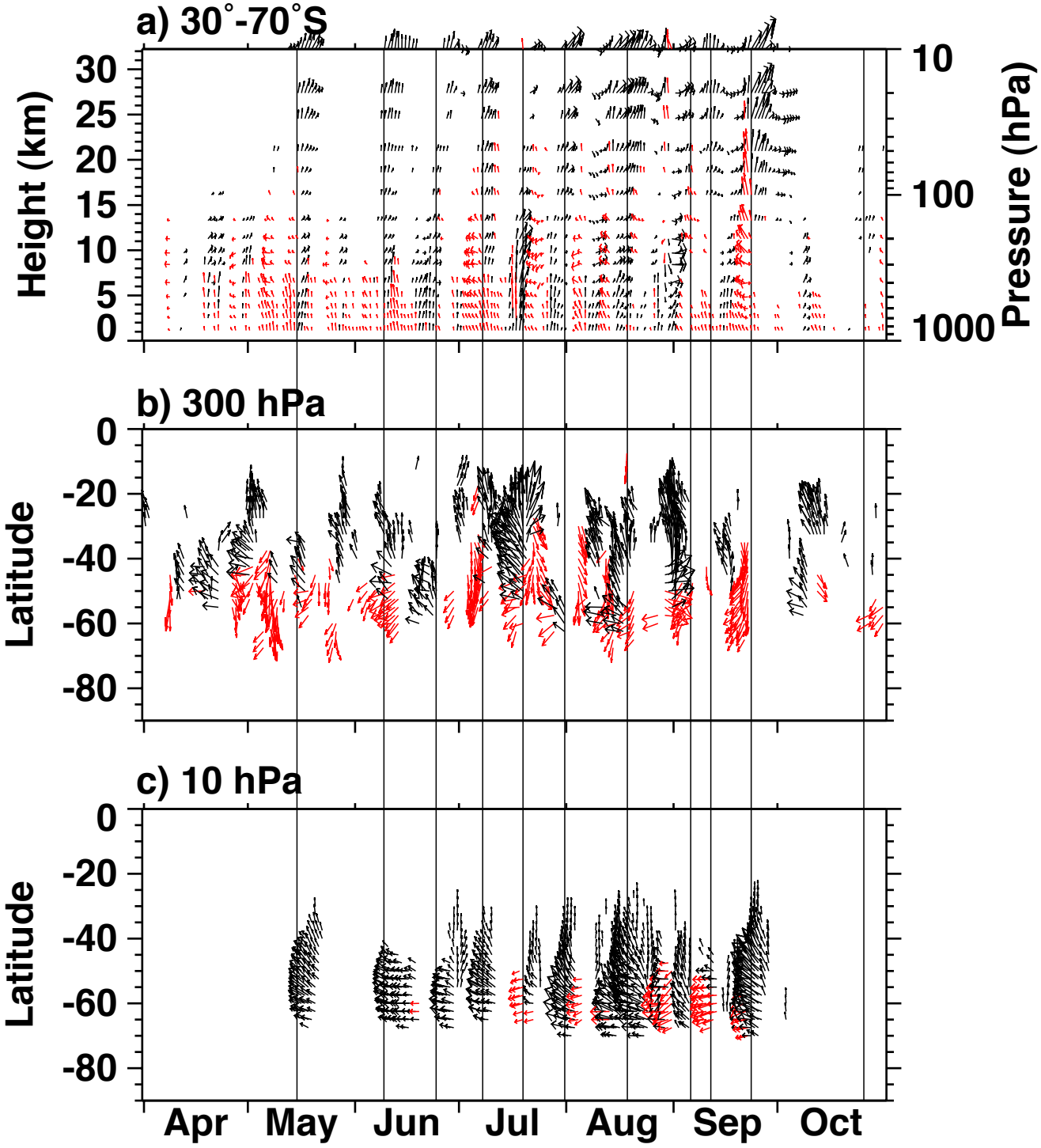


Figure 5. (a) Daily Eliassen-Palm (EP) flux vectors for waves 1–3 averaged from 30˚–70˚S. The vectors have been multiplied by the log of pressure to emphasize the lower altitude values. Vectors pointing up indicate vertical propagation while vectors pointing to the right indicate equatorward propagation. Daily EP flux vectors at 300 hPa (b) and 10 hPa (c). In these lower 2 panels, vectors pointing upward indicate equatorward propagation while vectors pointing to the left indicate upward propagation. In all 3 panels, EP flux vectors less than 20% of the maximum vector over the whole field have not been plotted. The colorscale used indicates black as equatorward pointing and red as poleward pointing.

# Newman & Nash: Figure 6

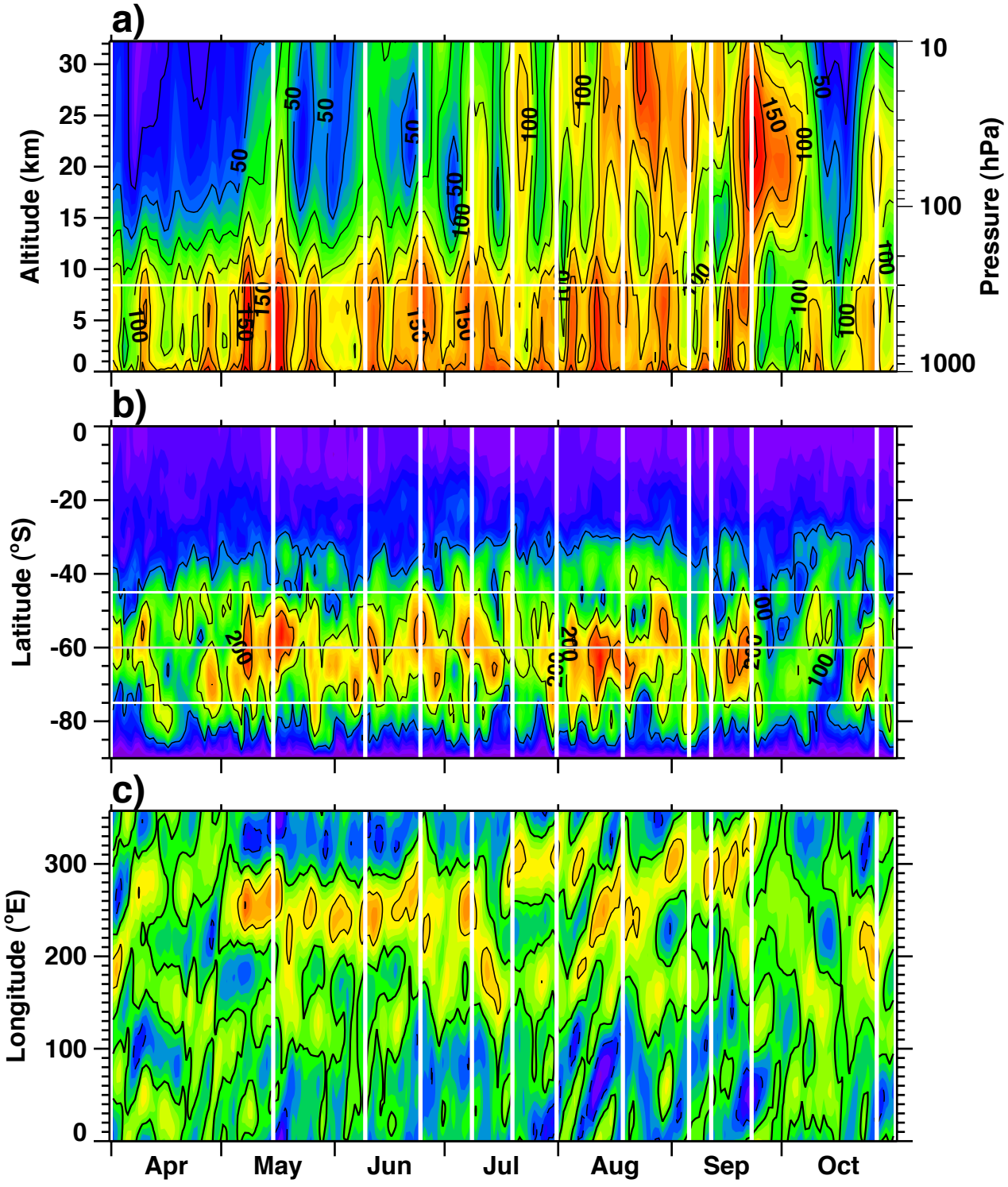


Figure 6. (a) Pressure-time plot of daily geopotential height rms waves 1–3 amplitude averaged over latitudes 45˚–75˚S. The rms wave amplitude is normalized by the density. The horizontal white line shows the 300-hPa level. Contour intervals are 25 m. (b) Latitude-time plot of daily geopotential height rms waves 1–3 amplitude at 300 hPa. The white horizontal lines indicate the 45˚ and 75˚S lines used in (a), while the horizontal gray line is the 60˚S line. Contour intervals are 100 m. (c) Longitude-time plot of daily geopotential height waves 1–3 deviations from the zonal mean at 60˚S and 300 hPa. Contour intervals are 300 m. The vertical lines passing through all panels indicate the days of maximum eddy heat flux at 100 hPa.

# Newman & Nash: Figure 7

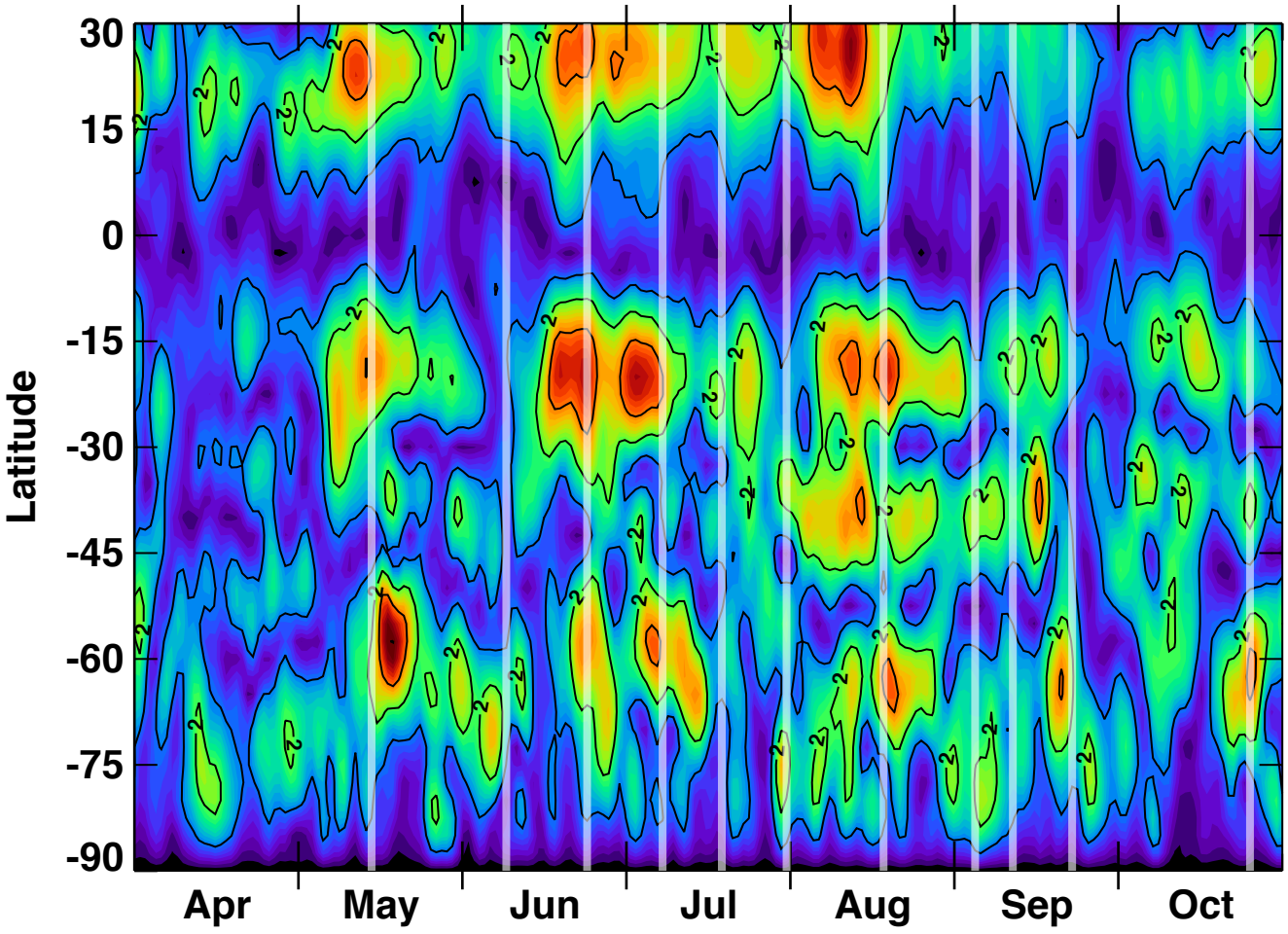


Figure 7. Latitude-time plot of the 300-hPa amplitude of wave 1 derived from the streamfunction. The streamfunction is derived from the nondivergent components of the wind field on pressure surfaces. The streamfunction values are normalized by the radius of the Earth. Units are m $s^{-1}$. The white semi-transparent vertical lines indicate the days of maximum eddy heat flux at 100 hPa.

Newman & Nash: Figure 8

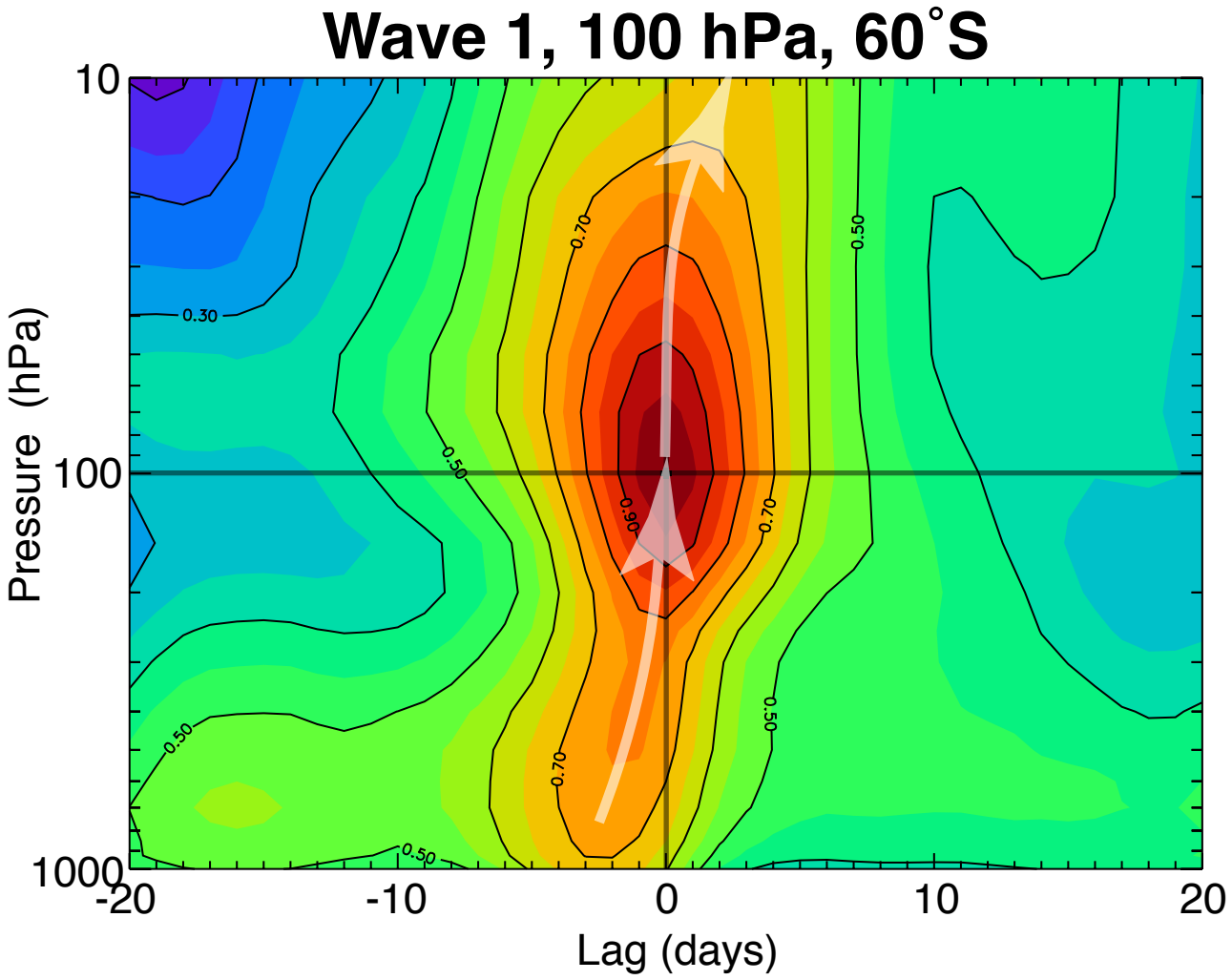


Figure 8. Contour plot of the 100 hPa, 60˚S wave 1 coherency plotted as a function of pressure and time lag. Coherency is similar to a correlation coefficient, and represents linearly related temporal variability between points. The white lines are drawn onto the axis of the maximum of the coherency to illustrate the vertical propagation of wave 1. Contour intervals are 0.1.

# Newman & Nash: Figure 9

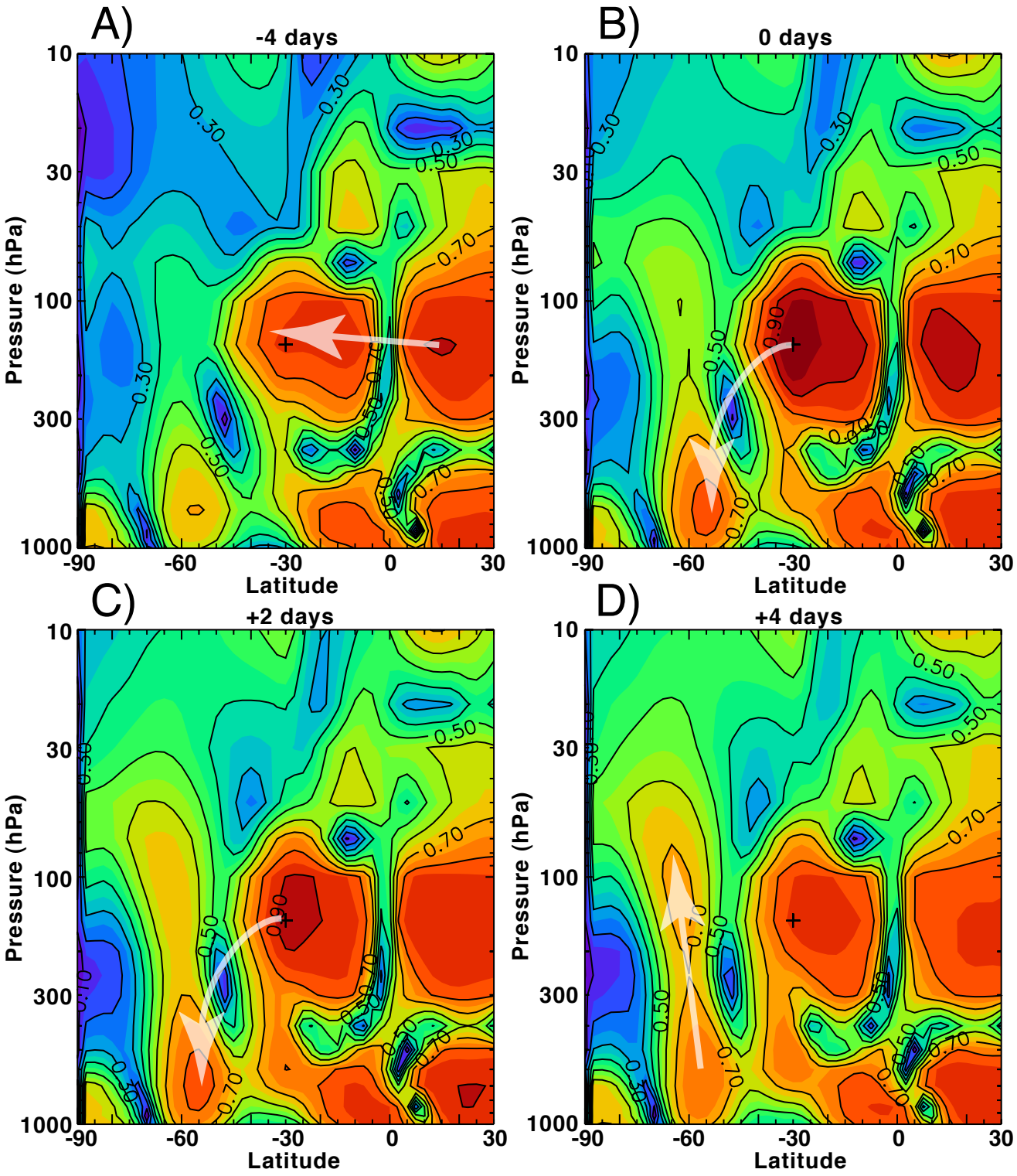


Figure 9. Contour plots of the 150 hPa, 30˚S wave 1 coherency plotted as a function of altitude and latitude for phase lags of (a) -4 days, (b) 0 days, (c) +2 days, and (d) +4 days. The white lines are drawn onto the axis of the maximum of the coherency to illustrate the propagation of wave 1. Contour intervals are 0.1.

# Newman & Nash: Figure 10

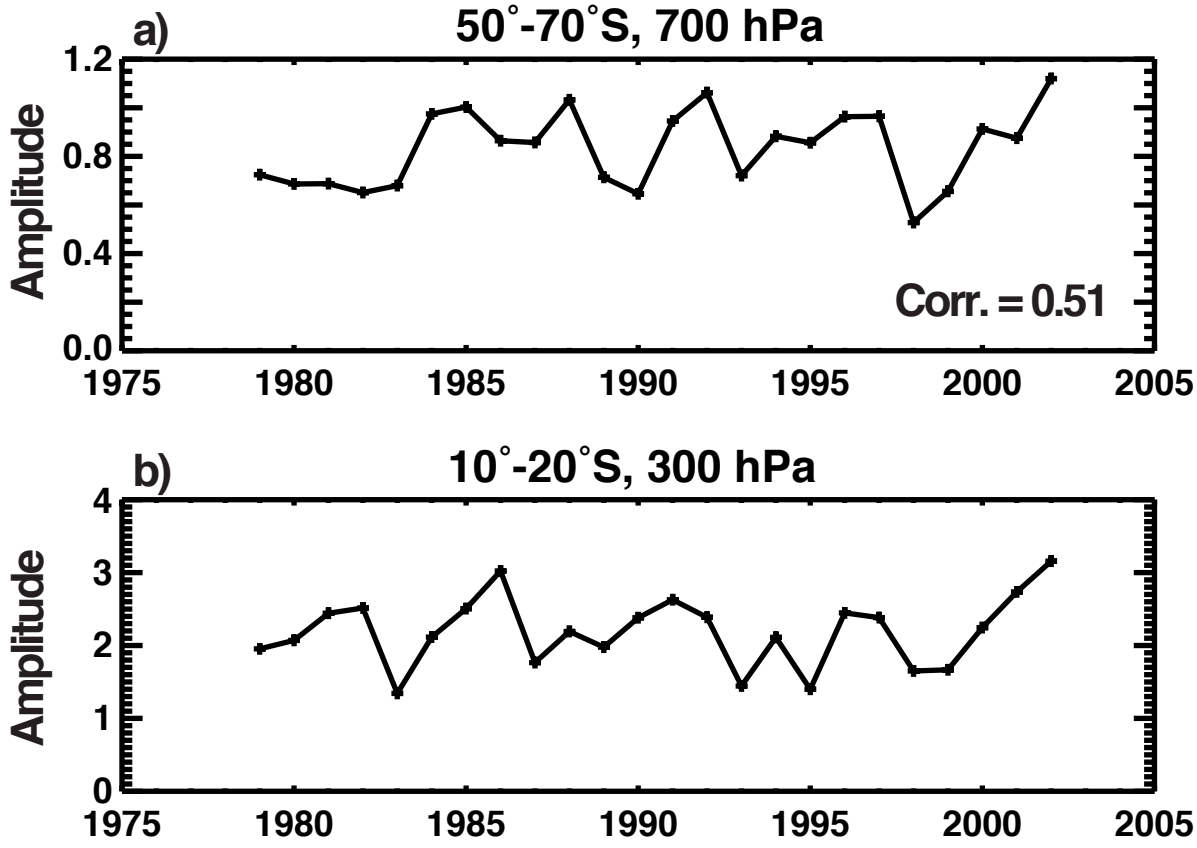


Figure 10. Amplitude of wave 1 streamfunction for 1979–2002 averaged over 1 May to 15 September for each year. (a) Streamfunction at 700 hPa and averaged for 50˚–70˚S. (b) Streamfunction at 300 hPa and averaged for 10˚–20˚S.The streamfunction is derived from the nondivergent part of the meridional and zonal winds on pressure surfaces.

# Newman & Nash: Figure 11

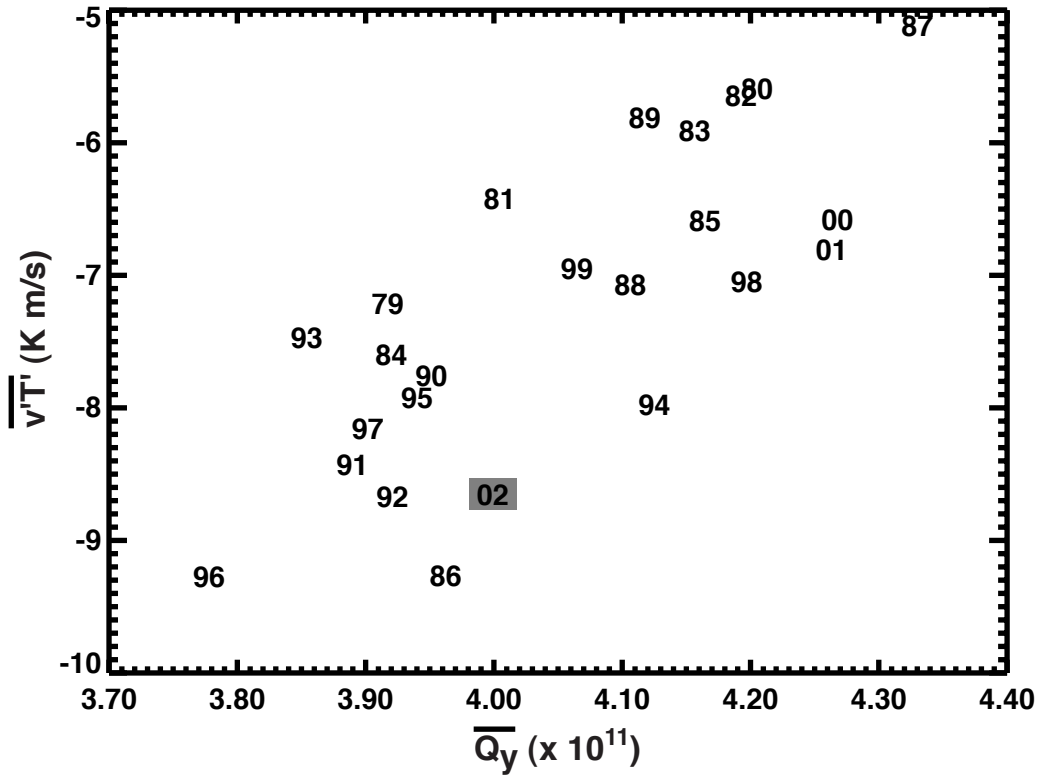


Figure 11. Eddy heat flux vs. the meridional gradient of the quasi-geostrophic potential vorticity ($Q_y$) averaged over 1 May to 15 September for each year. The heat flux is averaged for 45˚–75˚S at 100 hPa, while $Q_y$ is averaged for 40˚–60˚S and 100–400 hPa. The index of refraction is proportional to $Q_y$. The correlation is 0.55. Each year is indicated by the last two digits.